Lattice methods For Hadron Vacuum Polarisation in Muon $g-2$ Anomaly

20-21 Physics Tripos

May 2021

Candidate No. : 6963W
Supervisor : Dr. Bipasha Chakraborty

Abstract

This review is written to encourage more theoretical efforts on muon anomalous magnetic moment a_μ, particularly the Hadron Vacuum Polarisation (HVP) contribution, under Fermilab's recent announcement in 2021 April where an exacerbated 4.2σ deviation is observed between Standard Model theory and experiment. Current Lattice QCD methods including Hybrid Method and Time-Momentum Representation are established for HVP computation at leading order, and individual quark flavor contributions are examined along with their issues and remedies. Results for total $a_\mu^{HVP,LO}$ and flavor-specific contributions are compared between different lattice groups, and between lattice vs phenomenological routines. It is evident that current lattice study must be improved to a permile level precision to confront its phenomenological/experimental counterparts, and the focus shall be placed upon the improvement of statistical noise in dominant light-quark connected contribution.

Contents

1 Introduction

1.1 Muon $g-2$

Muon anomalous magnetic moment, denoted as a_μ, is one of the most delicate probes of new physics beyond Standard Model (SM), itself among the most precise quantities ever measured. The subject has earned considerable attention since 2004, the tantalizing E821 experiment result that is 3.2σ away from SM prediction [13]. In 2021 April, Fermilab announced its 1st run result - 4-fold improved in precision, when combined with E821 result a striking 4.2σ deviation from SM theory is observed. This exacerbated tension has urged investigation from both sides. While new experiments are planned at Fermilab and J-PARC, theoreticians are aiming to improve current theory from percent level to permile level for more a reliable SM prediction. One of such effort includes improving hadron vacuum polarisation contribution with lattice method, the subject of this review.

Muon magnetic moment μ can be written as:

$$\mu = g\frac{e}{2m_\mu}S$$

where g is the g-factor, predicted to be exactly 2 by Dirac's equation in quantum mechanics. However, quantum field theory suggests loop corrections that add onto the quantum mechanical prediction, hence $g \neq 2$. a_μ is defined as the fractional deviation of g from 2,

$$a_\mu = \frac{g-2}{2}$$

This is where the name '$g-2$' comes from.

Standard model predicts three types of loop corrections from Quantum Electrodynamics (QED), Electroweak theories (EW), and Quantum Chromodynamics (QCD) respectively, visualized in Figure 1. Formulated as

$$a_\mu^{SM} = a_\mu^{QED} + a_\mu^{EW} + a_\mu^{QCD}$$

a recent result [1] is quoted below:

$$a_\mu^{SM} = 116591810(43) \times 10^{-11}$$

with

$$a_\mu^{QED} = 116584718.931(104) \times 10^{-11}$$

$$a_\mu^{EW} = 153.6(1.0) \times 10^{-11}$$

$$a_\mu^{QCD} = 6923.7(53.4) \times 10^{-11}$$

a_μ^{QCD} has contribution from both **hadron vacuum polarisation** (HVP), the subject of this review, and **hadron light by light scattering** (HLbL), another important contribution that is thoroughly discussed in Section 4 and 5 in [1]:

$$a_\mu^{QCD} = a_\mu^{HVP} + a_\mu^{HLbL}$$

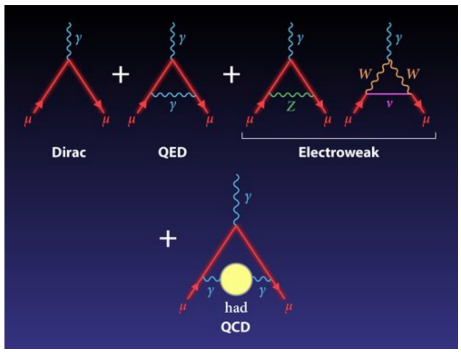

Figure 1: Example Feynman diagrams of all the contributions to g factor. The Dirac diagram is at the lowest level, giving $g = 2$. The rest are at one-loop level, involving a virtual photon (QED), virtual Z/$W^{\pm}$ (EW), or virtual hadron (QCD), giving the deviation from 2, a_μ. Diagrams in this figure are merely examples among all the possible diagrams that are not shown. Reprinted, see original source.

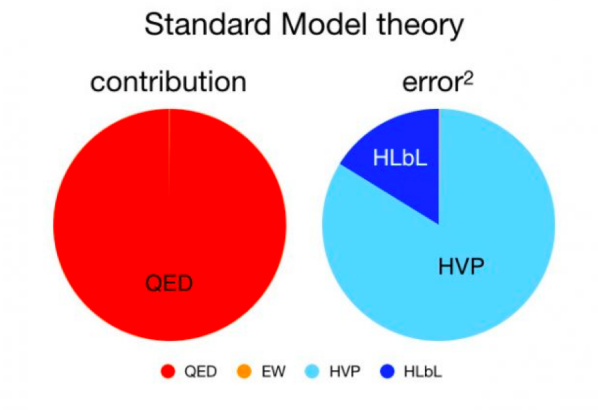

Figure 2: Pie charts displaying weight of different contributions in a_μ^{SM} and theoretical uncertainty. Reprinted, see original source.

The importance of QCD contribution, particularly HVP, is exemplified by the relative weight of different contributions as shown in Figure 2: Although a_μ^{QED} dominates in a_μ, theoretical uncertainties almost exclusively come from a_μ^{QCD}, and uncertainties from a_μ^{HVP} account for 70%. The high precision in QED and eletroweak parts is attributed to their perturbative construction, which is not completely plausible for QCD due to its non-perturbative features (i.e. color confinement). Therefore, to improve the SM estimation, one would necessarily confront the challenge of computing a_μ^{HVP}, the term dominating theoretical uncertainties.

1.2 Theoretical Efforts in HVP

a_μ^{HVP} can be either computed with **data-driven method**, or **lattice method**.

Data-driven method This method is based on a dispersive integral, i.e. at leading order (LO)

$$a_\mu^{\mathrm{HVP,LO}} = \frac{1}{4\pi^3}\int_{M_\pi^2}^{\infty} K(s)\sigma^0\left(e^+e^- \to \text{hadrons}(+\gamma)\right) ds \tag{1}$$

where the e^+e^-cross-section data σ^0 comes from experiments. K(s) is a kernel function. (See [1]) Therefore, this method is also termed as 'dispersive method' or 'phenomenology method' in literature. To compute the integral, cross-section of all the possible decay channels must be summed over. Alternative routine using τ decay cross-section is also possible, but is so far not precise enough for a_μ^{HVP} prediction. With this method, it's possible to compute $a_\mu^{HVP,NLO}$ (next leading order) and $a_\mu^{HVP,NNLO}$ (next-next leading order) with HVP iteration. See [1] for more details.

Lattice method This method features QCD calculation on a set of discretized spacetime points and extrapolation to continuum limit, shown in Figure 3. One can construct a 3+1 dimension spacetime lattice, quarks placed on lattice points with gluons connecting them like 'springs', resembling a crystal lattice.

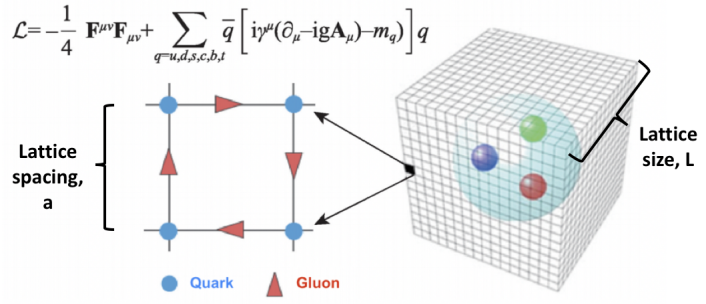

Figure 3: Graphic illustration of lattice QCD, with lattice spacing, a, and lattice size, L. Time dimension is not shown here. Reprinted, see original source.

One computes a_μ^{HVP} over this lattice and extrapolates the result to continuum, where the lattice is infinitely large and unit cell infinitely small. This method is shorthanded as 'LQCD', where 'L' stands for 'lattice'. It computes up to $a_\mu^{HVP,LO}$.

In this review, LQCD computations of $a_\mu^{HVP,LO}$ are established. Results are compared between different lattice groups and between lattice vs. phenomenology. All quantities are quoted in natural unit.

2 LQCD Methods for $a_\mu^{HVP,LO}$ Computation

In this section, prevalent lattice methods for $a_\mu^{HVP,LO}$ evaluations (**Hybrid Method** and **Time Momentum Representation**) are explained in general terms with their main issues and remedies. See more theoretical details in the referred publication.

Computation of $a_\mu^{HVP,LO}$ usually involves the HVP integral. This integral can be either done in Q^2 space, where Q is the reciprocal wave vector analogous to that in solid state physics, or in x_0 space, where x_0 is time in 4-vector formalism. Correspondingly, **Hybrid Method** computes the integral in Q^2 space while **Time Momentum Representation** does so in x_0 space.

2.1 Hybrid Method

The HVP integral is:

$$a_\mu^{\mathrm{HVP,LO}} = \left(\frac{\alpha}{\pi}\right)^2 \int_0^\infty dQ^2 f\left(Q^2\right) \hat{\Pi}\left(Q^2\right) \tag{2}$$

where

$$f\left(Q^2\right) = \frac{m_\mu^2 Q^2 Z^3\left(1 - Q^2 Z\right)}{1 + m_\mu^2 Q^2 Z^2}, \quad Z = -\frac{Q^2 - \sqrt{Q^4 + 4m_\mu^2 Q^2}}{2m_\mu^2 Q^2}$$

$$\hat{\Pi}\left(Q^2\right) \equiv 4\pi^2\left[\Pi(0) - \Pi\left(Q^2\right)\right]$$

$\Pi(Q^2)$ is the scalar vacuum polarisation tensor that can be constructed from electromagnetic current correlator $C_{\mu\nu}(x)$. [1]

The form of kernel $f(Q^2)$ suggests a divergence as $Q^2 \to 0$, which means the integrand peaks in low Q^2 region, signaling a difference in performance between low, intermediate, and high values of Q^2. The peak indicates dominance of low Q^2 region. However, this Q^2 region is far more noisy compared to high Q^2 region due to the finite size of lattice: analogous to a crystal lattice, the smallest wavevector is restrained to be $\frac{2\pi}{L}$ by L, the length of lattice. $Q < \frac{2\pi}{L}$ cannot be reached by lattice data. One has to extrapolate data into the unreachable region, introducing statistical and systematic uncertainties. Contrarily, high Q region can be very precisely determined perturbatively without lattice method.

The most important region being the least precise, the **Hybrid Method** was proposed to address this issue. It's a 'mixed' strategy that optimizes the computation by adopting different methods for different Q regimes. Two cuts are introduced at $Q^2_{low} \approx 0.1 Gev^2$ and $Q^2_{high} \approx 8 Gev^2$. The

integral is split into 3 parts:

$$
\begin{aligned}
a_\mu^{\mathrm{HVP,LO}} &= I_0 + I_1 + I_2 \\
I_0 &= \left(\frac{\alpha}{\pi}\right)^2 \int_0^{Q^2_{\mathrm{low}}} dQ^2 f\left(Q^2\right) \times \hat{\Pi}\left(Q^2\right) \\
I_1 &= \left(\frac{\alpha}{\pi}\right)^2 \int_{Q^2_{\mathrm{low}}}^{Q^2_{\mathrm{high}}} dQ^2 f\left(Q^2\right) \times \hat{\Pi}\left(Q^2\right) \\
I_2 &= \left(\frac{\alpha}{\pi}\right)^2 \int_{Q^2_{\mathrm{high}}}^{\infty} dQ^2 f\left(Q^2\right) \times \hat{\Pi}_{\mathrm{pert}}\ \left(Q^2\right)
\end{aligned}
\tag{3}
$$

I_0 covers the problematic low Q^2 region, and is approximated by either **fitting polynomials** or **time moments** (see Section 2.1.1 and 2.1.2). I_1 covers the intermediate Q^2 region which can be precisely calculated with lattice data and numerical integration. I_2 covers the high Q^2 region, computed with perturbation theory.

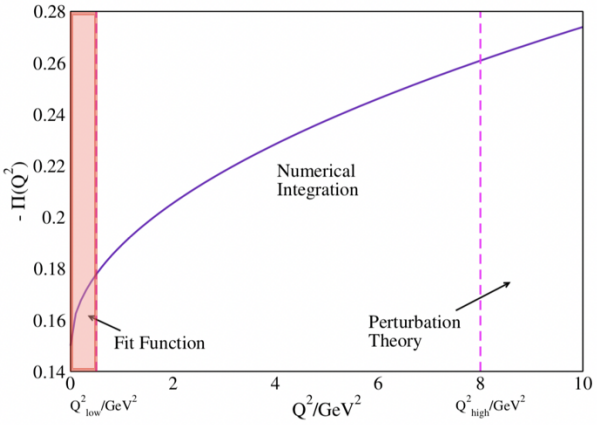

Figure 4: Illustration of hybrid method, with typical value of Q^2_{low} and Q^2_{high}. Reprinted from [1].

In general, the idea of a 'hybrid strategy' is very commonly used to address the variation in data performance across the interested region. This idea can also be seen in the **Window Method** (Section 2.2.1) and the design of **MUonE project** (Section 5).

2.1.1 Fitting Polynomials

As mentioned before, the most problematic part of the integral is I_0 for it being dominant but very uncertain. Analytic approximations are proposed to describe $\prod(Q^2)$ in low Q^2 region, including Padé functions [4] which states:

$$
\Pi_{[N,M]}\left(Q^2\right) = \Pi(0) + \frac{\sum_{i=1}^{N} a_i Q^{2i}}{1 + \sum_{i=1}^{M} b_i Q^{2i}} \tag{4}
$$

and conformal polynomials [12] which states:

$$
\Pi_N\left(Q^2\right) = \Pi(0) + \sum_{i=1}^{N} p_i w^i, \quad w = \frac{1 - \sqrt{1+z}}{1 + \sqrt{1+z}}, \quad z = Q^2/4M_\pi^2. \tag{5}
$$

Coefficients are found by fitting lattice data. To improve the stability of the fitting functions, one can supplement them with derivatives of $\Pi(0)$, estimated from either numerical differentiation or time moments.

2.1.2 Time Moments

Time moments [8] is analogous to Taylor expansion, hence are sometimes referred to as 'Taylor coefficients'. The essential idea is to expand $\Pi(Q^2)$ in terms of power of Q^2 (just like Taylor series), with the 'Taylor coefficients', namely the time moments, directly related to EM current correlator as shown below:

$$\Pi\left(Q^2\right) = \Pi_0 + \sum_{n=1}^{\infty} \Pi_n Q^{2n}$$

where

$$\Pi_0 = \Pi(0) = -\frac{1}{2}G_2, \quad \Pi_n = \frac{(-1)^{n+1}}{(2n+2)!}G_{2n+2}$$

$$G_{2n} \equiv \int_{-\infty}^{\infty} dx_0 x_0^{2n} C\left(x_0\right)$$

$$C\left(x_0\right) = -\frac{1}{3}\sum_{k=1}^{3}\int d^3x C_{kk}(x)$$

$C_{kk}(x)$ is the contraction of EM current correlator $C_{\mu\nu}(x)$ mentioned previously. Π_n is the nth time moment.

The advantages of computing time moments includes:

1. They can be used to construct Padé approximant or other approximants.
2. They are an intermediate result that can be used for comparison between different lattice groups, allowing for uncertainty investigation and cross checking.
3. They can also be constructed from experimental data, enabling comparison between data-driven method and lattice method.

2.2 Time Momentum Representation

Instead of doing the integral in Q^2 space, one can take $Q^\mu = (\omega, 0, 0, 0)$ and write the integral alternatively as:

$$a_\mu^{\mathrm{HVP,LO}} = \left(\frac{\alpha}{\pi}\right)^2 \int_0^{\infty} dx_0 C\left(x_0\right) \widetilde{f}\left(x_0\right) \tag{6}$$

which is an integral in Euclidean time. $\widetilde{f}\left(x_0\right)$ is a kernel function of form

$$\tilde{f}\left(x_0\right) = 8\pi^2 \int_0^{\infty} \frac{d\omega}{\omega} f\left(\omega^2\right)\left[\omega^2 x_0^2 - 4\sin^2\left(\frac{\omega x_0}{2}\right)\right]$$

This method is usually shorthanded as 'TMR'. [5]

The first issue arises due to the finite size of lattice again. Since the spacetime lattice is finite, the data it yields cannot reach infinite time. Therefore, beyond the furthest x_0 data point, one needs to extend the correlator into infinite time via approximation:

$$C(x_0) = \sum_{n=1}^{\infty} A_n \mathrm{e}^{-E_n x_0} \tag{7}$$

E_n is the energy of eigenstate $|n\rangle$ of the system. A_n is a matrix element associated with EM current. Eq. (7) is general form, and the specific form is model dependent. Since $C(x_0)$ depends on which eigenstates are present, detailed spectroscopic study must be conveyed to obtain a precise approximation.

The point x_0^{cut}at which one starts to replace correlator data with Eq. (7) is not only limited by the size of lattice, but also the deterioration of Signal-to-Noise ratio (StN) at large x_0. This is the second issue with TMR: the relative statistical uncertainty increases exponentially as x_0 increases, which brings down the precision. Thus, x_0^{cut} shall be neither too large for the overwhelming statistical noise to degrade the precision before reaching the cut, nor too small for the model dependence of correlator extrapolation to introduce extra uncertainties. Practically, x_0^{cut} is set to be $\geq$1.2 fm.

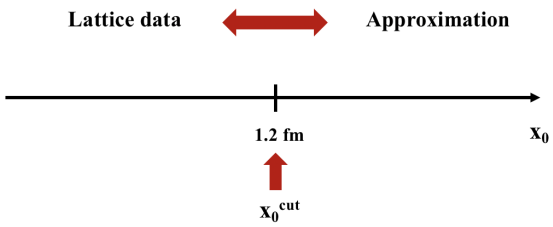

Figure 5: Illustration of time cut, as well as the methods adopted before and beyond cut.

2.2.1 Window Method

The aforementioned x_0-dependence of correlator performance encourages a 'splitting' of $a_\mu^{HVP,LO}$ into short (time) distance, intermediate 'window', and long distance parts, proposed by RBC/UKQCD collaboration[6]:

$$\begin{aligned}
a_\mu^{\mathrm{HVP,LO}} &= a_\mu^{\mathrm{SD}} + a_\mu^{\mathrm{W}} + a_\mu^{\mathrm{LD}} \\
a_\mu^{\mathrm{SD}} &= \left(\frac{\alpha}{\pi}\right)^2 \int_0^\infty dx_0 C(x_0) \widetilde{f}(x_0) \left[1 - \Theta(x_0, t_0, \Delta)\right] \\
a_\mu^{\mathrm{W}} &= \left(\frac{\alpha}{\pi}\right)^2 \int_0^\infty dx_0 C(x_0) \widetilde{f}(x_0) \left[\Theta(x_0, t_0, \Delta) - \Theta(x_0, t_1, \Delta)\right] \\
a_\mu^{\mathrm{LD}} &= \left(\frac{\alpha}{\pi}\right)^2 \int_0^\infty dx_0 C(x_0) \widetilde{f}(x_0) \Theta(x_0, t_1, \Delta)
\end{aligned} \tag{8}$$

where

$$\Theta\left(t, t', \Delta\right) = \left[1 + \tanh\left[\left(t - t'\right)/\Delta\right]\right]/2$$

Parameter Δ is used to smooth the boundaries, often set to be 0.15 fm. t_0 and t_1 define the boundaries of 'short distance' and 'long distance', taking values around 0.4 fm and 1.0 fm respectively. a_μ^{SD} is subjected to short distance effect such as discretization effect, while a_μ^{LD} is sensitive to the StN problem at long distance. In contrast, the intermediate window part a_μ^{W} is not as affected as these two, hence can be very precisely determined with lattice method.

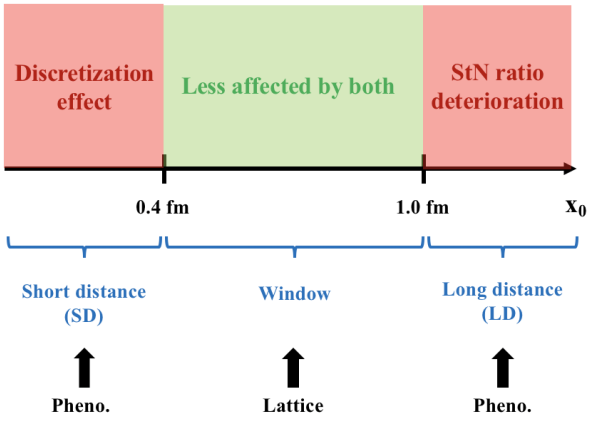

Figure 6: Illustration of window method.

Similar to hybrid method, **Window Method** suggests a 'hybrid' way to determine $a_\mu^{HVP,LO}$ by keeping the precise lattice computation of intermediate window while replacing the problematic a_μ^{SD} and a_μ^{LD} with data-driven computations, which gives a final result more precise than using LQCD or data-driven method alone.

The advantages of window construction includes:

1. They are an intermediate result that can be used for comparison between different lattice groups, just like time moments.

2. They can also be constructed with experimental R-ratio data via

$$C\left(x_0\right) = \frac{1}{12\pi^2}\int_0^\infty d(\sqrt{s})R(s)se^{-\sqrt{s}x_0}$$

   and substitution back to Eq. (6). This allows comparison and even combination of lattice and data-driven method.

Concluding this section, the two routines described above are essentially the same apart from integrating over different domains. However, this means that if the statistical uncertainty presents in one method, it manifests as well in the other. In fact, as mentioned TMR suffers a statistical noise at large Euclidean time, and this issue manifests in time moments too where one loses statistical precision in higher order time moments (as n increases for Π_n).

3 Individual Quark Contributions in $a_\mu^{HVP,LO}$

For hadron vacuum polarization, two types of Feynnman diagrams are available: **quark-line connected** (quark connected) and **quark-line disconnected** (quark disconnected). [14]

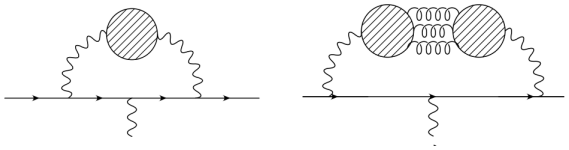

Figure 7: Cartoon depicting connected and disconnected contribution. In a connected diagram, a pair of virtual quarks is generated and annihilates into a photon, whereas in a disconnected diagram the virtual quark pair annihilates into gluons. Reprinted from [14]

The quark connected contribution can be decomposed into individual quark contributions since the EM current correlator sums over all quark flavors. [1]This means we can write

$$a_\mu^{\mathrm{HVP,LO}} = a_{\mu,\mathrm{conn}}^{\mathrm{HVP,LO}} + a_{\mu,\mathrm{disc}}^{\mathrm{HVP,LO}} \tag{9}$$

and

$$a_{\mu,\mathrm{conn}}^{\mathrm{HVP,LO}} = a_\mu^{\mathrm{HVP,LO}}(ud) + a_\mu^{\mathrm{HVP,LO}}(s) + a_\mu^{\mathrm{HVP,LO}}(c) + a_\mu^{\mathrm{HVP,LO}}(b), \tag{10}$$

Therefore, to obtain total quark connected contribution, one computes individual quark contributions and sums up all. In practical, different quark flavors have different statistical and systematic uncertainties, hence must be computed separately. The quark disconnected contribution must also be evaluated for total $a_\mu^{HVP,LO}$.

3.1 Methodology

Connected Contributions Connected contributions from different flavors can be found in more or less the same way. Many lattice groups have adopted TMR method: one find the $C(x_0)$ for one specific quark flavor, say f, and substitute it back to Eq. (6) to get the individual quark connected contribution $a_{\mu,conn}^{HVP,LO}(f)$. For details, see [11]. Alternatively, for each quark flavor one could find the time moments to construct Padé approximants, then do the HVP integral Eq. (2), as explained in [8]. A combination of both routines is possible.

An important clarification needs to be made about the treatment of u and d quark - they are treated together in isospin symmetry by all the lattice groups when calculating $a_\mu^{HVP,LO}$, which assumes they have identical mass. This is why in Eq. (10) they are combined into one single contribution and termed as 'light-quark contribution'. The effects caused by their physical difference in mass and charge are studied in 'Isospin Breaking effects' (IB), leading to a small yet non-negligible correction around $7.2(3.4) \times 10^{-10}$.[1] In this review, isospin symmetry $m_u = m_d$ is assumed.

Disconnected Contribution Usually, disconnected contribution is also computed with TMR. One finds the electromagnetic current, performs Wick contraction to obtain the disconnected correlator, then substitutes back into the HVP integral. A more detailed description of this method can be found in Appendix D, [15].

3.2 Connected *ud* Contribution

The term $a_{\mu,conn}^{HVP,LO}(ud)$, or light-quark contribution, accounts for 90% of $a_{\mu,conn}^{HVP,LO}$, hence is the most important part. Meanwhile, it is also known to be notoriously noisy and suffering from many uncertainties.

As mentioned, to compute this contribution, one could either adopt TMR or use time moments and Padé approximants. The main lattice groups involved and the methods they adopted are summarized in the table below [1]:

Method	Group(s) involved
TMR	BMW
	UKQCD
	ETM
	Mainz
	Aubin et al.
moments	HPQCD
both	Fermilab-HPQCD-MILC

Table 1: Groups computing light-quark contribution and their methods.

3.2.1 Issues and Remedies

The main issues with this calculation include **statistical** and **systematic** uncertainties. Statistical uncertainty is related to the 'random noises' in data, while systematic uncertainties are artifacts of lattice configuration - finite size of lattice gives *finite volume effect*, and finite spacing of lattice sites gives *discretization effect*.

Statistical uncertainty Statistical uncertainty mainly refers to the StN problem, where the signal-to-noise ratio in correlator $C(x_0)$ deteriorates at large Euclidean time - a typical issue with TMR. Those groups who employed time moments need to deal with the same issue but in a different manifestation, as described at the end of Section 2.
Two types of remedies are proposed: 'fitting' and 'bounding'. The 'fitting' solution is to replace the noisy region with a fit based on smaller x_0 data. Groups adopting this strategy include Mainz,

ETM, HPQCD, and Fermilab. The replacement typically starts at 2-2.5 fm. The 'bounding' solution, instead of giving a prediction, introduces a cut x_cut beyond which the data is replaced with an upper and lower bound. x_cut is usually around 3 fm. Groups adopting this strategy include BMW, UKQCD, and Aubin et al.

Systematic uncertainty: finite volume effect Often short-handed as 'FVE', this is a lattice artifact that is related to the size of lattice, L. It can be addressed with chiral perturbation theory (ChPT) at NLO (next to leading order) and NNLO (next next to leading order). A systematic study of FVE can be found in [11] and [10] where $a_{\mu,conn}^{HVP,LO}(ud)$ results are compared between lattice configurations that are same except for lattice size. A detailed NLO calculation can be found in [2] and a NNLO calculation is given in [3]. In fact, the NNLO contribution is not negligible - it is roughly 50% of NLO contribution with the same sign.

Systematic uncertainty: discretization effect This mainly refers to an uncertainty that is at order $O(a)$, where a is the lattice spacing. It is an artifact coming from a finite lattice spacing. Dependence on finite lattice spacing varies for different lattice formulations, thus one must study this effect accordingly based on the specific lattice configuration involved. For this reason, its origin will not be further elaborated here. It is usually treated with ChPT. To mitigate such uncertainty, one may conduct a fitting as described in Appendix B, [7].

3.3 Connected *s, c, b* Contribution

$a_{\mu,conn}^{HVP,LO}(s)$ accounts for $\sim$ 8% of $a_{\mu,isosym}^{HVP,LO}$, and $a_{\mu,conn}^{HVP,LO}(c)$ $\sim$2%. $a_{\mu,conn}^{HVP,LO}(b)$ contributes by only 0.04%, which is nearly negligible at current precision level.

For b and c contribution, they don't suffer FVE and StN problems as much as the ud case, therefore the dominating uncertainty is discretization effect. Besides, since b and c data can be easily extracted experimentally, they can be evaluated with data-driven method and compared with the lattice result. Current lattice result agrees well with phenomenological ones.

For s contribution, the StN problem is slightly worse than b and c, but the correlator can still be determined accurately at larger numerical cost. FVE effect is fairly small [8], hence the dominating uncertainty is discretization effect as well.

3.4 Disconnected Contributions

As mentioned in Section 3.1, disconnected contribution is usually done in TMR. However, it is also possible to derive $a_{\mu,disc}^{HVP,LO}$ based on ChPT as mentioned in [9]. Its upper bound is found to be 2% of the total $a_{\mu}^{HVP,LO}$ value, which means it is not negligible for a permile precision goal.

The biggest challenge for this contribution comes from statistical noises. For more detailed explanations and remedies, see [1].

4 Results

4.1 Total $a_\mu^{HVP,LO}$ Results

Collaboration	N_f	$a_\mu^{\mathrm{HVP,LO}} \times 10^{10}$	Fermion	$\hat{\Pi}(Q^2)$
ETM-18/19	2+1+1	692.1 (16.3)	tmQCD	TMR
FHM-19	2+1+1	699 (15)	HISQ	Padé w. Moments/TMR
BMW-17	2+1+1	711.1 (7.5)(17.5)	Stout4S	TMR
HPQCD-16	2+1+1	667 (6)(12)	HISQ	Padé w. Moments
ETM-13	2+1+1	674 (21)(18)*	tmQCD	VMD
Mainz/CLS-19	2+1	720.0 (12.4)(9.9)	Clover	TMR
PACS-19	2+1	737 (9)$(^{+13}_{-18})$	StoutW	TMR/Padé
RBC/UKQCD-18	2+1	717.4 (16.3)(9.2)	DWF	TMR
Mainz-17	2	654 (32)$(^{+21}_{-23})$*	Clover	TMR
KNT-19	pheno.	692.8 (2.4)	–	dispersion
DHMZ-19	pheno.	694.0 (4.0)	–	dispersion
BDJ-19	pheno.	687.1 (3.0)	–	dispersion
FJ-17	pheno.	688.1 (4.1)	–	dispersion
RBC/UKQCD-18	lat.+pheno.	692.5 (1.4)(2.3)	DWF	TMR + disp.

Table 2: Summary of all the groups involved in the comparison and their methodology. N_f indicates which quarks are included in the sea quark setting of simulation: 2+1+1 all included, 2+1 c quark missing, 2 s and c both missing. 'Fermion' shows which specific model is assumed for the fermions. [1]

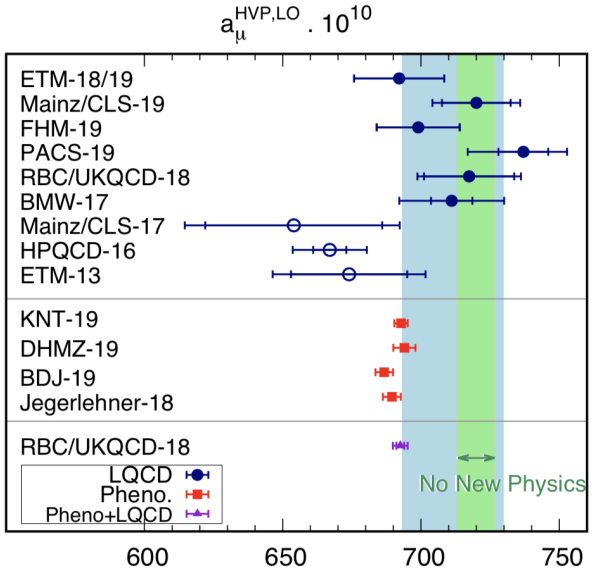

Figure 8: Plot of results from previous table. Blue band indicates the range of latest world average result. Green band refers to the zone where theoretical results are consistent with experiments. [1]

Results from the recently active groups and their methodologies [1] are tabulated in Table 2, including lattice groups and phenomenology groups (those working with data-driven method).

Their results for total $a_\mu^{HVP,LO}$ is plotted in Figure 8.

Mainz/CLS-17, HPQCD-16 and ETM-13 are older efforts that have already been superseded. They are consistent with each other, but are in mild tension with the most up-to-date results. It is evident that results from BMW, RBC/UKQCD, and Mainz/CLS agree well, suggesting 'no new physics' scenario. ETM and FHM results agree with each other, but are at 1σ tension from BMW, RBC/UKQCD, and Mainz/CLS. PACS result is 1σ away from the three 'no new physics' results and 2σ from ETM and FHM. These six results are combined to form a 'lattice world average',

$$a_\mu^{HVP,LO} = 711.6(18.4) \times 10^{-10}$$

which is represented by the blue band. From the phenomenology side, data-driven results are fairly consistent with each other, and they all lie on the border of blue band, indicating a mild 1σ tension between lattice and data-driven method.

From the graph, one also observes that the uncertainties reported by different lattice groups are similar in order of magnitude, and they much larger than those of data-driven method. Thus, the 'mild' tension between these two methods must be interpreted discreetly - it is probably not a sign of agreement, but merely a consequence of the large uncertainty in lattice methods.

To summarize, lattice results are generally in agreement within a spread of 2σ, and a 1σ tension is suspended between lattice and data-driven results. The most recent lattice world average is found to be $a_\mu^{HVP,LO} = 711.6(18.4) \times 10^{-10}$. Uncertainties in lattice method is around 2.6%, at subpercent level, while data-driven method uncertainties is around 0.5%, at permile level. Therefore, an improvement to permile precision is necessary for lattice method to form a conclusive comparison with data-driven method.

4.2 Individual Quark Contribution Results

To investigate the deviation among total $a_\mu^{HVP,LO}$ results, it is instructive to compare the results of individual quark contributions. Groups involved and their results [1] are tabulated and plotted in Table 3 and Figure 9.

Light-quark Light-quark results display a spread similar to that of total results. Given the dominance of this contribution, it's likely to be the reason for the spread in total $a_\mu^{HVP,LO}$. For $N_f = 2 + 1 + 1$ configuration, a 1σ spread is seen. This is presumably caused by the different strategies implemented to resolve the StN issue mentioned earlier.

Collaboration	N_f	$a_\mu^{\mathrm{HVP,LO}}(ud)\times 10^{10}$	$a_\mu^{\mathrm{HVP,LO}}(s)\times 10^{10}$	$a_\mu^{\mathrm{HVP,LO}}(c)\times 10^{10}$	$a_{\mu,\mathrm{disc}}^{\mathrm{HVP,LO}}\times 10^{10}$
ETM-18/19	2+1+1	629.1(13.7)	53.1(1.6)(2.0)	14.75(42)(37)	–
Aubin *et al.*-19	2+1+1	659 (22)	–	–	–
FHM-19	2+1+1	637.8(8.8)	–	–	−13(5)
BMW-17	2+1+1	647.6(7.5)(17.7)	53.73(04)(49)	14.74(04)(16)	−12.8(1.1)(1.6)
HPQCD-16	2+1+1	599.0(6.0)(11.0)†	–	–	0(9)(−)
HPQCD-14	2+1+1/2+1	–	53.41(00)(59)	14.42(00)(39)	–
Mainz/CLS-19	2+1	674(12)(5)	54.5(2.4)(0.6)	14.66(45)(6)	−23.2(2.2)(4.5)
PACS-19	2+1	673(9)(11)	52.1(2)(5)	11.7(0.2)(1.6)	–
RBC/UKQCD-18	2+1	649.7(14.2)(4.9)	53.2(4)(3)	14.3(0)(7)	−11.2(3.3)(2.3)
Mainz/CLS-17	2	588.2(31.7)(16.6)	51.1(1.7)(0.4)	14.3(2)(1)	–

Table 3: Summary of individual quark results from different groups.

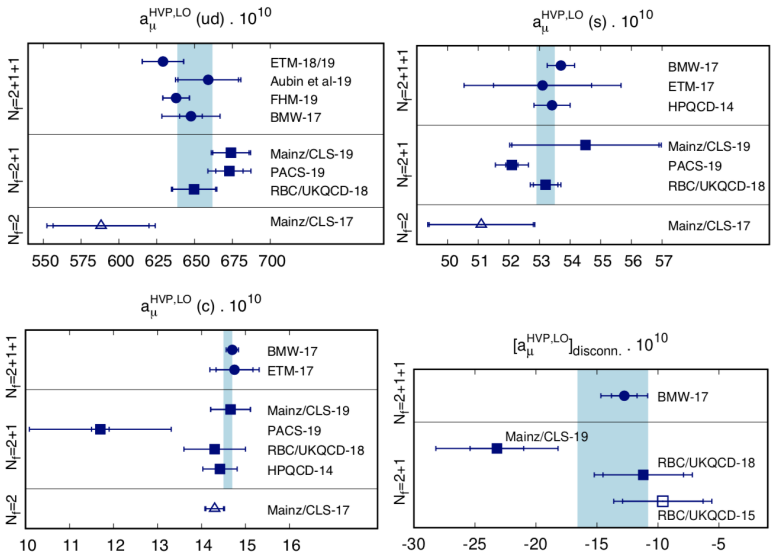

Figure 9: Plot of results from previous table. Blue band indicates the range of latest world average result.

s and c For these two flavors, the $N_f = 2+1+1$ configuration results agree well. So are $N_f = 2+1$ ones except for PACS. As mentioned, these two flavors suffer most from discretization effect, and PACS has a lattice artifact at $O(a)$ that is not seen in other groups, which explains the deviation. Besides, the much larger uncertainty in ETM and Mainz results are statistical in nature, and can be solved by further computational efforts.

Quark disconnected More results are required this computation. From the plot, current results agree within 1σ, except for Mainz. This is due to one of the fit ansätze it adopted. See [1].

5 Conclusion and Outlook

In this review, lattice QCD calculation of hadron vacuum polarization has been established from first principle. Comparison of total $a_\mu^{HVP,LO}$ results between different lattice groups and lattice vs data-driven shows that:

1. Lattice results are in agreement, despite a spread of 2σ.
2. Data-driven method results are consistent with each other.
3. A mild tension exists between lattice and data-driven results. Lattice method must be improved to permile level precision for future comparison.

Comparison between individual flavors reveals:

1. The spread in total $a_\mu^{HVP,LO}$ could be attributed to light-quark contribution, where the spread is caused by different strategies to cope with StN problems.
2. More computational effort is needed for disconnected part.

These comparisons consolidated the necessity of a permile level precision goal. Future lattice work shall proceed with a focus on lowering the statistical uncertainty in dominating ud contribution, while improving the IB correction precision. It would be ideal if each lattice group can walk through the routines of others and produce more results for comparison.

Last but not least, exciting intermix between lattice and phenomenological/experimental effort is upcoming to bring more insights on the matter: phenomenologists may apply lattice method for IB correction in their alternative τ decay routine, which might yield a result precise enough as an independent check against current mainstream results. Moreover, a new experimental project MUonE at CERN has been proposed to help measure the low Q^2 region which bothers LQCD studies. A hybrid mode of 'experimental+LQCD+pertubation' will optimize the uncertainty budget and boost precision.

It is doubtless that after decades of theoretical, experimental, and phenomenological efforts, we would expect the veil of new physics to be soon revealed upon muon $g-2$, another forthcoming triumph of physics.

References

[1] T. Aoyama et al. "The anomalous magnetic moment of the muon in the Standard Model". In: *Physics Reports* 887 (Dec. 2020), pp. 1–166. ISSN: 0370-1573. DOI: 10.1016/j.physrep.2020.07.006. URL: http://dx.doi.org/10.1016/j.physrep.2020.07.006.

[2] Christopher Aubin et al. "Finite-volume effects in the muon anomalous magnetic moment on the lattice". In: *Physical Review D* 93.5 (Mar. 2016). ISSN: 2470-0029. DOI: 10.1103/physrevd.93.054508. URL: http://dx.doi.org/10.1103/PhysRevD.93.054508.

[3] Christopher Aubin et al. "Light quark vacuum polarization at the physical point and contribution to the muon g2". In: *Physical Review D* 101.1 (Jan. 2020). ISSN: 2470-0029. DOI: 10.1103/physrevd.101.014503. URL: http://dx.doi.org/10.1103/PhysRevD.101.014503.

[4] Christopher Aubin et al. "Model-independent parametrization of the hadronic vacuum polarization andg-2 for the muon on the lattice". In: *Physical Review D* 86.5 (Sept. 2012). ISSN: 1550-2368. DOI: 10.1103/physrevd.86.054509. URL: http://dx.doi.org/10.1103/PhysRevD.86.054509.

[5] David Bernecker and Harvey B. Meyer. "Vector correlators in lattice QCD: Methods and applications". In: *The European Physical Journal A* 47.11 (Nov. 2011). ISSN: 1434-601X. DOI: 10.1140/epja/i2011-11148-6. URL: http://dx.doi.org/10.1140/epja/i2011-11148-6.

[6] T. Blum et al. "Calculation of the Hadronic Vacuum Polarization Contribution to the Muon Anomalous Magnetic Moment". In: *Physical Review Letters* 121.2 (July 2018). ISSN: 1079-7114. DOI: 10.1103/physrevlett.121.022003. URL: http://dx.doi.org/10.1103/PhysRevLett.121.022003.

[7] Bipasha Chakraborty et al. "Hadronic vacuum polarization contribution to a from full lattice QCD". In: *Physical Review D* 96.3 (Aug. 2017). ISSN: 2470-0029. DOI: 10.1103/physrevd.96.034516. URL: http://dx.doi.org/10.1103/PhysRevD.96.034516.

[8] Bipasha Chakraborty et al. "Strange and charm quark contributions to the anomalous magnetic moment of the muon". In: *Physical Review D* 89.11 (June 2014). ISSN: 1550-2368. DOI: 10.1103/physrevd.89.114501. URL: http://dx.doi.org/10.1103/PhysRevD.89.114501.

[9] C. T. H. Davies et al. "Hadronic-vacuum-polarization contribution to the muon's anomalous magnetic moment from four-flavor lattice QCD". In: *Physical Review D* 101.3 (Feb. 2020). ISSN: 2470-0029. DOI: 10.1103/physrevd.101.034512. URL: http://dx.doi.org/10.1103/PhysRevD.101.034512.

[10] M. Della Morte et al. "A lattice calculation of the hadronic vacuum polarization contribution to (g - 2) μ". In: *EPJ Web of Conferences* 175 (2018). Ed. by M. Della Morte et al., p. 06031. ISSN: 2100-014X. DOI: 10.1051/epjconf/201817506031. URL: http://dx.doi.org/10.1051/epjconf/201817506031.

[11] D. Giusti, F. Sanfilippo, and S. Simula. "Light-quark contribution to the leading hadronic vacuum polarization term of the muon g2 from twisted-mass fermions". In: *Physical Review D* 98.11 (Dec. 2018). ISSN: 2470-0029. DOI: 10.1103/physrevd.98.114504. URL: http://dx.doi.org/10.1103/PhysRevD.98.114504.

[12] Maarten Golterman, Kim Maltman, and Santiago Peris. "New strategy for the lattice evaluation of the leading order hadronic contribution to(g2)". In: *Physical Review D* 90.7 (Oct. 2014). ISSN: 1550-2368. DOI: 10.1103/physrevd.90.074508. URL: http://dx.doi.org/10.1103/PhysRevD.90.074508.

[13] Fred Jegerlehner and Andreas Nyffeler. "The muon g2". In: *Physics Reports* 477.1-3 (June 2009), pp. 1–110. ISSN: 0370-1573. DOI: 10.1016/j.physrep.2009.04.003. URL: http://dx.doi.org/10.1016/j.physrep.2009.04.003.

[14] Christoph Lehner et al. "Opportunities for Lattice QCD in quark and lepton flavor physics". In: *The European Physical Journal A* 55.11 (Nov. 2019). ISSN: 1434-601X. DOI: 10.1140/epja/i2019-12891-2. URL: http://dx.doi.org/10.1140/epja/i2019-12891-2.

[15] M. Della Morte et al. "The hadronic vacuum polarization contribution to the muon g 2 from lattice QCD". In: *Journal of High Energy Physics* 2017.10 (Oct. 2017). ISSN: 1029-8479. DOI: 10.1007/jhep10(2017)020. URL: http://dx.doi.org/10.1007/JHEP10(2017)020.